Stochastic analog to phase transitions in chaotic coupled map lattices

Francisco Sastre* and Gabriel Pérez†
Departamento de Física Aplicada, Centro de Investigación y de Estudios Avanzados del Instituto Politécnico Nacional, Unidad Mérida, Apartado Postal 73 ''Cordemex,'' 97310 Mérida, Yucatán, Mexico
(Received 22 December 2000; published 14 June 2001)

Stochastic dynamical systems are shown to exhibit the same order-disorder phase transitions that have been found in chaotic map lattices. Phase diagrams are obtained for diffusively coupled two-dimensional (2D) lattices, using two stochastic maps and a chaotic one, for both square and triangular geometries, with simultaneous updating. We show how the use of triangular geometry reduces (or even eliminates) the reentrant behavior found in the phase diagrams for the square geometry. This is attributed to the elimination (via frustration) of the antiferromagnetic clusters common to simultaneous updating of square lattices. We also evaluate the critical exponents for the stochastic maps in the triangular lattices. The strong similarities in the phase diagrams and the consistency between the critical exponents of one stochastic map and the chaotic one, evaluated in an early work by Marcq *et al.* [Phys. Rev. Lett. **77**, 4003 (1996); Phys. Rev. E **55**, 2606 (1997)] suggest that the ''sign-persistence,'' defined as the probability that the local map keeps the sign of the local variable in one iteration, plays a fundamental role in the presence of continuous phase transitions in coupled map lattices, and is a basic ingredient for models that belong to this weak Ising universality. However, the fact that the second stochastic map, which has an extremely simple local dynamics, seems to fall in the 2D Ising universality class, suggests that some minimal local complexity is also needed to generate the specific correlations that end up giving non-Ising critical behavior.

DOI: 10.1103/PhysRevE.64.016207 PACS number(s): 05.45.Ra, 05.70.Fh, 64.60.Cn

I. INTRODUCTION

The study of extended chaotic systems, defined by ensembles of interacting simple elements whose local dynamics are chaotic, is one of the most exciting new areas in nonlinear dynamics. Within this field one of the problems that has been attracting much interest lately is the appearance of nontrivial collective behavior in coupled map lattices (CMLs), beginning with the collective oscillations found by Chaté and Manneville [2] in lattices of diffusively coupled cellular automata. CMLs are the simplest models for the study of spatiotemporal chaos, and can be used to simulate the cooperative behavior found in many biological, computational, physical, chemical, and even social systems [3]. Some types of chaotic CMLs present order-disorder transitions with the same phenomenology found in continuous phase transitions (PTs) in equilibrium statistical mechanics. In particular, a very interesting example was found by Miller and Huse (MH) [4], for two-dimensional (2D) lattices of odd-symmetric piecewise-linear chaotic maps, with diffusive coupling. These transitions occur between two globally chaotic states, and the largest Lyapunov exponent remains continuous in the critical point [5]. The symmetry and dimensionality of the local maps are those of the Ising model, and using very general arguments, an Ising-like behavior was expected [6]. In fact, this order-disorder PT was initially located in the 2D Ising universality class, but extensive calculations for this and similar models [1] indicate that the transition does not fit entirely there, the main difference being in the critical exponent for the correlation length (ν), whose value was found to be 0.887(18) [number(s) between parentheses corresponds to the uncertainty in the last digit(s) of the quantity], clearly differing from the Ising value ($\nu=1$). These results were obtained with simultaneous updating of lattice sites, while an asynchronous updating of the same model recovered the critical exponents of the 2D Ising class. Recent evaluations of critical exponents on Toon cellular automata lattices [7] have also found non-Ising exponents, giving $\nu=0.85(2)$, but with discrepancies in the ratios γ/ν and β/ν with respect to both the 2D Ising model and the MH lattice model.

It seems obvious that for this order-disorder PT, the diffusive coupling is the factor that gives the global order, while the chaotic local evolution provides for the disorder. In a sense, one takes the diffusion as analogous to the ferromagnetic coupling in an Ising model, while the local chaos acts as a source of ''thermal fluctuations'' (a temperature). The picture however, is not really as simple. Maps that are similar to that used by Miller and Huse may or may not present continuous PTs [1,8,9], and moreover, two different maps with the same local Lyapunov exponent (i.e., with the same degree of chaoticity) present different critical points [9]. It is clear, therefore, that an extra factor is needed to understand the origin of these PTs. Looking again to the MH dynamics, one finds that two of its fundamental characteristics are that it has a uniform invariant distribution, and that it shows a tendency for the local variable to keep its sign under iteration. Following this lead, in this work we show an alternative way of studying local dynamics that gives continuous PTs in diffusive lattices, by making them completely stochastic, preserving the mentioned behavior. Specifically, we use stochastic processes with uniform invariant distributions, and with a certain probability that the local variable keeps the same sign in the next time iteration. We call this quantity the

*Electronic address: sastre@kin.cieamer.conacyt.mx
†Electronic address: gperez@kin.cieamer.conacyt.mx

sign-persistence of the map. We then implement numerical simulations of the CMLs with local stochastic maps, our goal being to compare both systems (deterministic and stochastic) in order to check how close to each other their behaviors are; in other words, to see if they fall in the same universality class. We made this comparison through the construction of the phase diagram for three CMLs, one chaotic, named the generalized Miller-Huse (GMH) map, and two stochastic, named threshold and density maps, and the evaluation of critical exponents for the stochastic maps (the critical exponents for the MH map and similar models were evaluated in Ref. [1]). Here we implement finite-size scaling (FSS) analysis of the results in the standard way used in equilibrium statistical mechanics.

Additionally, we want to cover two additional details in the behavior of the MH model, details that were pointed out originally by Marcq *et al.* [1]. First, after growing from zero on crossing the critical coupling, the order parameter starts to decrease as the coupling approaches its maximum value of 1, and second, antiferromagnetic looking domains appear in the lattice. These two features go clearly against what one expects of a diffusive system, since after all the coupling is intended to be of a ferromagnetic nature, and is assumed to homogenize the state of the lattice. We will put these effects in the context of a reentrance behavior found for both the chaotic and the stochastic models. We will show that the introduction of frustration, via the use of triangular lattices, reduces reentrance and even eliminates it completely for one case.

This article is organized as follows. In Sec. II we give the definitions of the two stochastic maps, we also give the definitions of the equivalent thermodynamics variables. These are the same ones given in previous works [1,9]. In Sec. III we present the phase diagrams for square and triangular lattices in the GMH, threshold, and density maps. Section IV is dedicated to FSS and the results of the critical exponents for the stochastic maps. In Sec. V we discuss our results.

II. MODELS AND DEFINITIONS

In a previous work [9] we introduced a *generalized Miller-Huse* map

$$\phi(y)=\begin{cases} 2y/(\alpha-1)+(\alpha+1)/(\alpha-1) & \text{for} \quad -1\leqslant y\leqslant -\alpha, \\ y/\alpha & \text{for} \quad -\alpha<y<\alpha, \\ 2y/(\alpha-1)-(\alpha+1)/(\alpha-1) & \text{for} \quad -1\leqslant y\leqslant -\alpha, \end{cases} \tag{2.1}$$

from where one gets the MH map setting $\alpha=1/3$. This family of maps has uniform invariant distributions, and the sign persistence can be easily evaluated, giving

$$p=\frac{1+\alpha}{2}. \tag{2.2}$$

The first stochastic map introduced, the *threshold map*, is closely related to the GMH map and is defined by

$$\phi(y)=\begin{cases} \operatorname{sgn}(y)r & \text{for} \quad |y|<p, \\ -\operatorname{sgn}(y)r & \text{for} \quad |y|>p, \end{cases} \tag{2.3}$$

where the sign persistence p is the internal parameter, and r is a uniformly distributed random number within [0,1]. Figure 1 shows the GMH and the threshold maps with the same value of p. The second stochastic map used, the *density map*, is defined by

$$\phi(y)=\begin{cases} \operatorname{sgn}(y)r & \text{with probability} \quad p, \\ -\operatorname{sgn}(y)r & \text{with probability} \quad 1-p, \end{cases} \tag{2.4}$$

where we have assigned directly the sign persistence in the dynamics (see Fig. 2).

The 2D coupled system was implemented using the discrete evolution rule given by

$$y_{\mathbf{r}}^{t+1}=(1-\epsilon)\,\phi(y_{\mathbf{r}}^{t})+\frac{\epsilon}{N_n}\sum_{\langle \mathbf{r}'\rangle}\phi(y_{\mathbf{r}'}^{t}); \tag{2.5}$$

here $\mathbf{r}$ indicates position in the lattice, t is the iteration counter (the discrete time), $\langle \mathbf{r}'\rangle$ indicates sum over nearest neighbors, N_n is the number of nearest neighbors, and $\phi(y)$ is the local map (GMH, threshold, or density). This gives us the desired simultaneous updating of all lattice sites. The instantaneous order parameter m_L^t is defined by

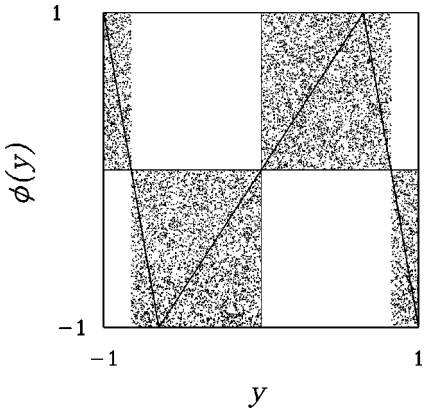

FIG. 1. GMH (solid line) and threshold map (points). In both cases we have $p=0.825$.

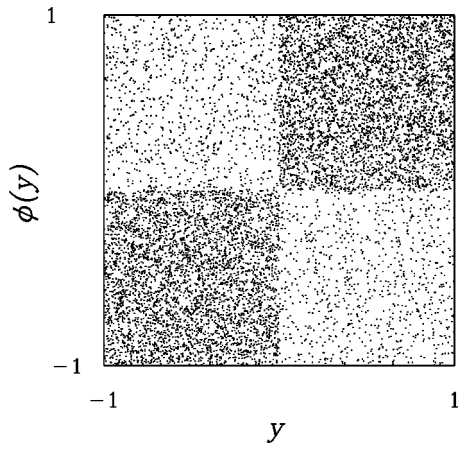

FIG. 2. Density map with $p=0.825$.

$$m_L^t=\frac{1}{N}\sum_{\mathbf{r}} y_{\mathbf{r}}^t, \tag{2.6}$$

where $N=L^2$ is the number of lattice sites, and the sum is over all lattice sites. The order parameter is obtained by taking, after letting a suitable transient time pass, the time average of the last quantity

$$M_L=\langle m_L\rangle=\frac{1}{T}\sum_{t=1}^{T}|m^t(L)|. \tag{2.7}$$

Here T is the time interval over which the average is taken. The susceptibility used in this work is defined by

$$\chi_L=N\langle(|m_L^t|-M_L)^2\rangle. \tag{2.8}$$

Finally, for the evaluation of critical points and other uses, we also compute the fourth order cumulant [10]

$$U_L=1-\frac{M_L^{(4)}}{3(M_L^{(2)})^2}, \tag{2.9}$$

where $M_L^{(n)}=\langle m_L^n\rangle$. As the control parameter (the coupling parameter, the sign persistence, or a combination of both quantities) tends to a critical point, one finds that $U(L)\rightarrow U^*$, where U^* is independent of the size of the system. This gives a good estimator for the critical points, just by getting the crossing point for different lattice sizes. We will discuss more about cumulant properties in Sec. IV.

III. PHASE DIAGRAMS AND REENTRANCES

We begin by computing the complete phase diagrams for the GMH and the threshold maps, in square lattices, as a function of the coupling ϵ and the sign persistence p. We worked with relatively small lattices (up to $L=40$), which gave us a good relation between accuracy and computational cost. These phase diagrams are shown in Fig. 3, and their almost exact coincidence for most of the parameter space is evident, substantiating our assertion that a fundamental factor for the appearance of MH-type PTs in diffusive chaotic lattices is the sign persistence. In fact, the coincidence in the phase diagrams is such that one is tempted to assert that the deterministic nature of the MH map is irrelevant for its collective behavior: all that matters is the distribution of signs it gives on iteration. However, results obtained for the density map indicate that this would be an oversimplification, as will be discussed in the conclusions. The region where this coincidence is lost is that of very large p values, where we can go from a disordered phase to an ordered one, and then back to a disordered phase, as we increase ϵ. We also observe this behavior in the phase diagram for the density map (Fig. 4), although the ordered phase appears for larger values of p. This reentrance seems to be due to the development of small antiferromagnetic domains, as can be observed in Fig. 5, where we show snapshots for three points (one for each region, with $L=48$) for the threshold map. One can clearly observe the presence of antiferromagnetic domains in the second and third snapshots. A similar behavior is observed in the GMH map. This means then that already in the ordered phase some antiferromagnetic clustering starts to develop, and that this phenomenon becomes so prevalent that it destroys the ferromagnetic order. It is important to remark that

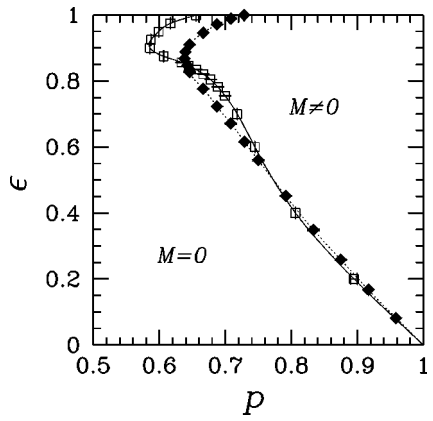

FIG. 3. Phase diagram for square lattices. Filled marks and dotted line are for the threshold map; open marks and solid line are for the GMH map. In both systems a reentrance can be observed for large values of the coupling. Lines are splines for visualization.

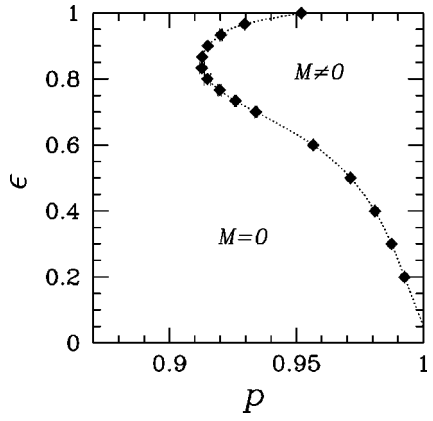

FIG. 4. Phase diagram for the density map in square lattices. A behavior analogous to that of the GMH and threshold maps can be observed. In this case the phase transition is present for large values of p.

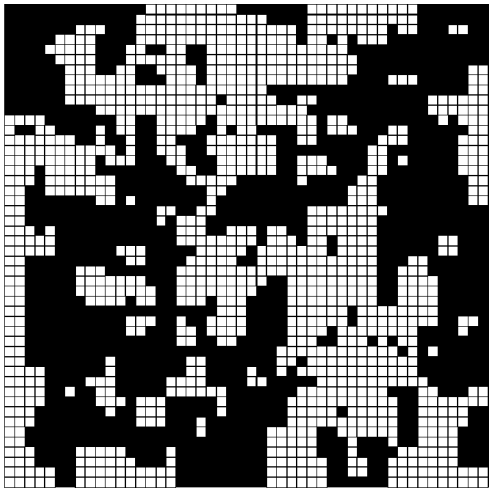

(a)

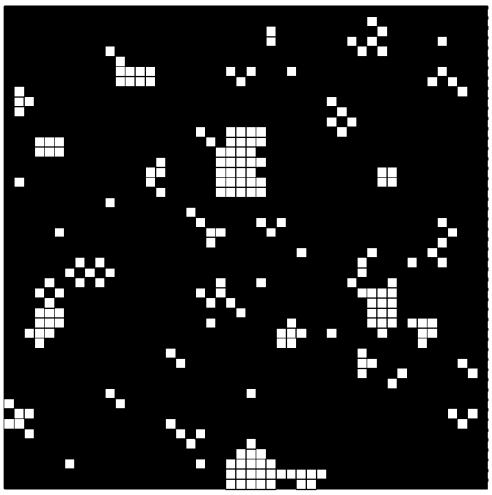

(b)

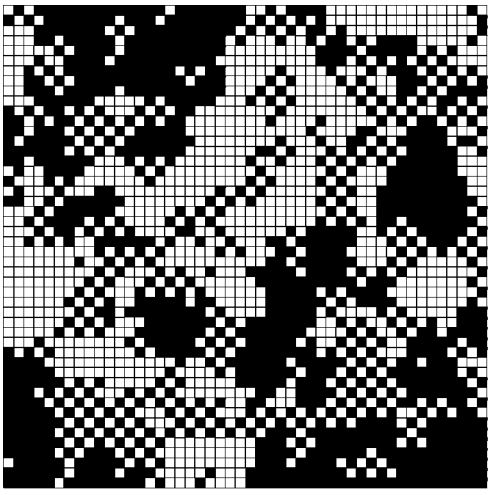

(c)

FIG. 5. Snapshots for the threshold map with $L=48$ in square lattices for (a) disordered phase ($\epsilon=0.6$), (b) ordered phase and ($\epsilon=0.875$) and (c) second disordered phase ($\epsilon=0.975$). We can observe that small antiferromagnetic domains begin to appear in the ordered phase. The sign persistence is fixed at $p=0.66$ for the three cases.

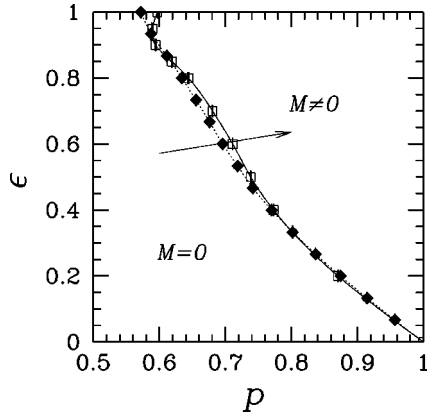

FIG. 6. Phase diagram for triangular lattices. Filled marks and dotted line are for the threshold map; open marks and solid line are for the GMH map. The reentrance disappears for the threshold map, and almost disappears for the GMH map. Lines are splines for visualization. The arrow shows the line along which the critical exponents were evaluated.

for the systems considered here a fully developed antiferromagnetic phase has not been found. These antiferromagnetic clusters crop in other ferromagnetic models, when simultaneously updated [11]; a fascinating anecdotical report of this problem was given recently by Hayes [12].

In a similar way to what happens in the Ising and other equilibrium models, one can discourage the appearance of antiferromagnetic behavior via frustration. To see what effect this has on the reentrance, we have calculated the phase diagrams for the three maps in triangular lattices. The results obtained are shown in Figs. 6 and 7, where we can observe that, as expected, the reentrance disappears for the threshold map (snapshots for this system are shown in Fig. 8). There is a very significant reduction of the reentrance in the GMH and the density maps. Again, we get almost perfect coincidence in the phase boundary between the GMH and the threshold maps, except for the high coupling region. As is normal with an increase on the coordination of the lattice,

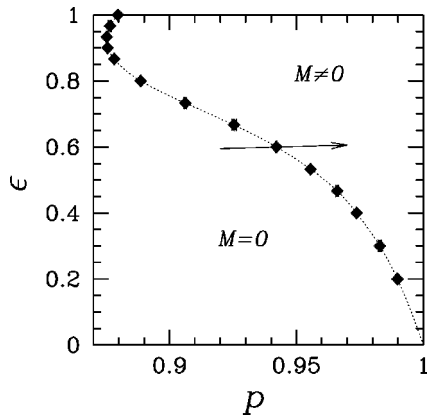

FIG. 7. Phase diagram for the density map in triangular lattices. A behavior analogous to that of the GMH and threshold maps can be observed. In this case the reentrance gets reduced, but does not disappear. The arrow shows the line along which the critical exponents were evaluated.

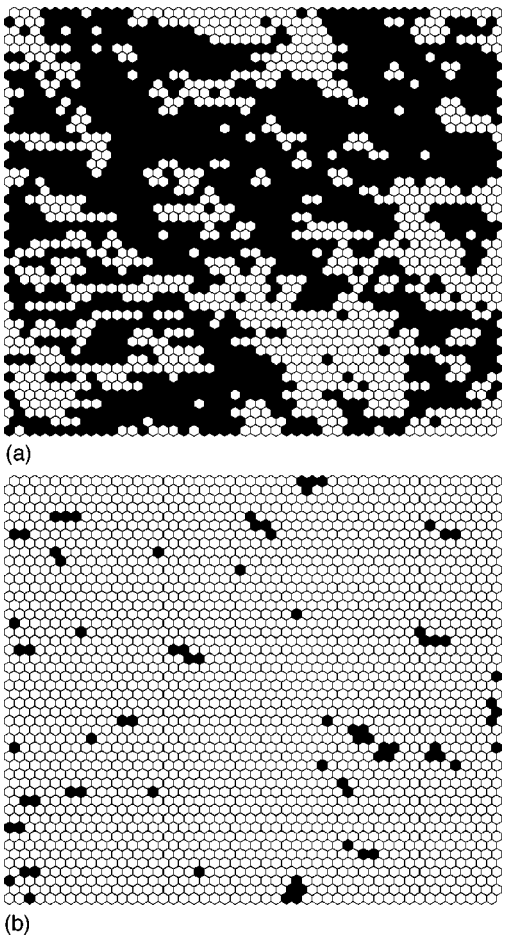

FIG. 8. Snapshots for the threshold map with $L=48$ in triangular lattices for (a) disordered phase ($\epsilon=0.6$), (b) ordered phase ($\epsilon=0.9$). Here we do not have a second disordered phase. The sign persistence is fixed at $p=0.66$ for both cases.

phase boundaries shift towards smaller values of the coupling. We then may assert that the appearance of antiferromagnetic clusters is strongly correlated with the reentrance. The results mentioned up to now clarify why the map called f_5 in Ref. [8] did not show any PT: it had a sign persistence of 0.6 on a square lattice, and in this regime the reentrance may allow one to cover the full 0-1 coupling range without crossing the phase boundary (Fig. 3).

IV. EVALUATION OF CRITICAL EXPONENTS

Up to now we have seen that the behavior of the phase boundaries for the stochastic maps we are proposing, and for the chaotic GMH map, are very similar. To make the equivalence in the global behavior between these different dynamical systems complete, that is, to find if they belong in the same universality class, we need to evaluate the critical exponents for the stochastic maps, and compare with the ones found for the MH and similar maps [1,7]. We evaluated the critical exponents ν, β, and γ for the threshold and the density maps in triangular lattices. This geometry was chosen over the square one, on account of previous indications that the presence of antiferromagnetic domains may introduce undesirable correlations that end up requiring large finite-size corrections in the evaluation of critical exponents. In order to handle just one control variable, we carried out this evaluation along a line approximately perpendicular to the phase boundary, using the parametrizations $p=0.6+0.2g$, $\epsilon=0.572+0.064g$ for the threshold map and $p=0.92+0.05g$, $\epsilon=0.5949+0.011g$ for the density map. In both cases the control parameter is g.

Starting with the basic postulation for the free energy at equilibrium FSS (without irrelevant operators)

$$F(T,B,L)=L^{-d}\hat{F}(|T-T_c^{\infty}|L^{1/\nu},BL^{(\beta+\gamma)/\nu}), \tag{4.1}$$

it is possible to get the FSS relations for the different thermodynamic quantities, interpreting g as the control parameter. In particular, it can be shown that the fourth order cumulant U, the magnetization M, and the susceptibility χ behave in the critical region as

$$U_L(g)=\hat{U}(L^{1/\nu}(g-g_c)), \tag{4.2}$$

$$M_L(g)=L^{-\beta/\nu}\hat{M}(L^{1/\nu}(g-g_c)), \tag{4.3}$$

$$\chi_L(g)=L^{\gamma/\nu}\hat{\chi}(L^{1/\nu}(g-g_c)), \tag{4.4}$$

where g_c is the critical point in the thermodynamic limit. (For a general review of FSS theory see Ref. [13].)

In order to find the critical point we used the standard crossing-of-cumulants method, implemented via minimization of the sum of the square distances between the cumulant curves for different lattice sizes. These curves were fitted using polynomial approximations, choosing the degree of the polynomial that gives the lowest χ^2 for degree of freedom. Once a value for g_c is obtained, the critical exponents have been evaluated using the relations [1,14]

$$\begin{gathered}\partial_g U_L(g_c)\sim L^{1/\nu},\\ \partial_g \log M_L(g_c)\sim L^{1/\nu},\\ \partial_g \log M_L^{(2)}(g_c)\sim L^{1/\nu},\\ M_L(g_c)\sim L^{-\beta/\nu}\\ M_L^{(s)}(g_c)\sim L^{-\beta/\nu}\\ \chi_L(g_c)\sim L^{\gamma/\nu},\end{gathered} \tag{4.5}$$

where $M_L^{(s)}(g)=\sqrt{M_L^{(2)}(g)}$, and the derivatives were evaluated using the best (in the sense of lowest χ^2 for degree of freedom) polynomial fitting for each curve.

A. Critical exponents for the threshold map

For this map we worked with eight lattice sizes, from $L=34$ to $L=120$. Here we got

$$g_c=0.481\,67(17),$$

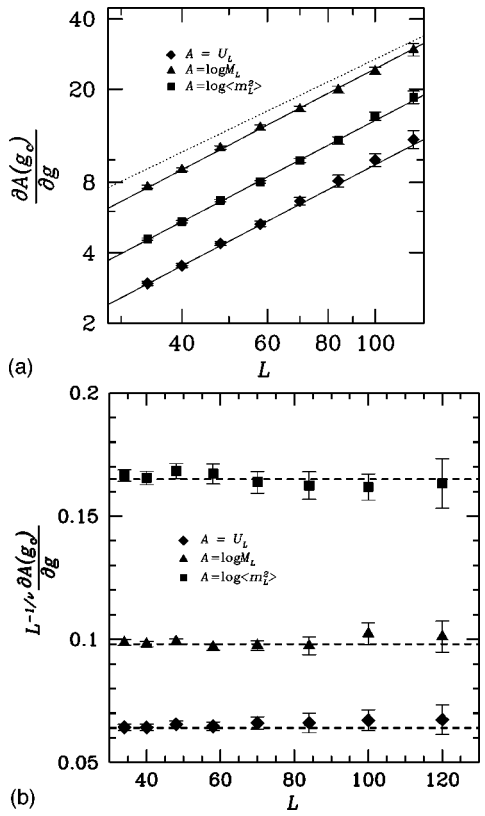

FIG. 9. Direct measure of the critical exponent ν for the threshold map. (a) Log-log graph, solid lines correspond to $\nu=0.921$, and the dotted line gives the 2D Ising value ($\nu=1$). (b) The same graph in a linear scale. Scaling corrections for this case were not necessary.

which translates into $p=0.696\,334(34)$ and $\epsilon=0.602\,827(11)$ for the particular point we choose in the phase boundary. It was found that ν and γ/ν did not need finite-size corrections for the range of L values used, while β did. In Fig. 9 we show, as an example, the direct measure of the correlation length exponent ν for the threshold map. The values obtained were $\nu=0.921(22)$, and $\gamma/\nu=1.741(11)$. In the β/ν case, scale corrections had to be introduced [1,13]. Although FSS allows for an infinity of correction exponents, associated with the irrelevant couplings of the model, it is customary to use just one effective exponent, associated with the dominant corrections, since this is usually the reliability limit for numerical fitting. For the quantities that we are considering here, the critical behaviors with effective corrections are given as

$$\partial_g U_L(g_c)\simeq L^{1/\nu}(A_0+A_1L^{-\omega}),$$

$$\partial_g \log M_L(g_c)\simeq L^{1/\nu}(B_0+B_1L^{-\omega}),$$

$$\partial_g \log M_L^{(2)}(g_c)\simeq L^{1/\nu}(C_0+C_1L^{-\omega}),$$

$$M_L(g_c)\simeq L^{-\beta/\nu}(D_0+D_1L^{-\omega}), \tag{4.6}$$

$$M_L^{(s)}(g_c)\simeq L^{-\beta/\nu}(E_0+E_1L^{-\omega}),$$

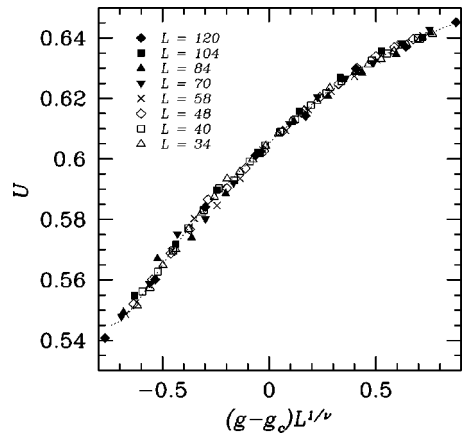

FIG. 10. Data collapse for the cumulant curves in the threshold map. The critical coupling found was $g_c=0.481\,70(4)$. The dotted line is the polynomial fitting.

$$\chi_L(g_c)\simeq L^{\gamma/\nu}(F_0+F_1L^{-\omega}).$$

Where A_0, A_1, B_0, etc. are nonuniversal real parameters and ω is a nonuniversal effective correction exponent that is different for each critical exponent. For the threshold map, we found $\beta/\nu=0.1257(43)$, with a correction exponent $\omega=9.4(5)$.

We also verified the results for ν using the collapse of the different cumulant curves. This was accomplished by fitting all the different values of $U_L(g)$ to the universal form given in Eq. (4.2), using a nonlinear minimization of χ^2. The results are shown in Fig. 10; the values obtained for the nonlinear parameters of the fit were $g_c=0.481\,70(4)$, and $\nu=0.926(7)$, completely consistent with the ones given before.

B. Critical exponents for the density map

For this case we worked with seven lattice sizes, from $L=34$ to $L=104$; we followed the same protocol of that in the threshold map. The critical point was located at

$$g_c=0.447\,14(28),$$

which gives $p=0.942\,357(14)$ and $\epsilon=0.599\,819(3)$. We are presenting the example of the direct measure for ν in Fig. 11. From this graph we observe that it is necessary to implement scale corrections in this case, although the deviation from the straight line is mild. The critical exponents β and γ were obtained without the inclusion of scale corrections. The values obtained were $\nu=1.027(8)$ with an effective correction exponent $\omega=5.7(9)$, $\beta/\nu=0.1255(20)$, and $\gamma/\nu=1.749(9)$.

As for the previous map, we checked the results using a direct collapse of the cumulant curves. The values obtained for the nonlinear parameters in the fit were $g_c=0447\,15(18)$, which is in perfect agreement with the value given above, and $\nu=0.981(11)$. It should be noticed that no finite-size corrections were used for the collapse, which explains the disagreement between this value and that obtained before. The results of this collapse are given in Fig. 12.

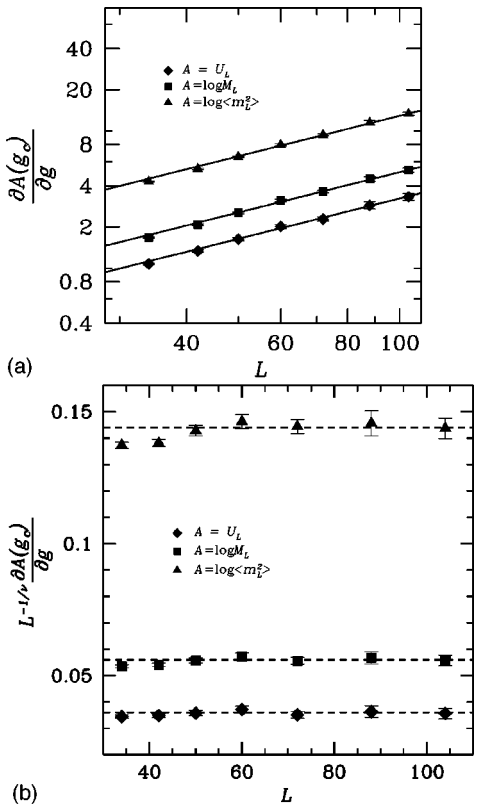

FIG. 11. Direct measure of the critical exponent ν for the density map. (a) Log-log graph, with $\nu=1.024$. (b) The same graph in a linear scale. Here the scale corrections are necessary.

V. CONCLUSIONS

In this work we have shown a stochastic map that reproduces quite closely the behavior found for a continuous, piecewise-linear odd-symmetric chaotic map, when it is embedded in diffusively coupled regular lattices. In particular, the critical behavior is fundamentally the same. This relation appears even though the only similarities between the two models are that both have uniform invariant distributions, and that their sign persistencies have been made equal.

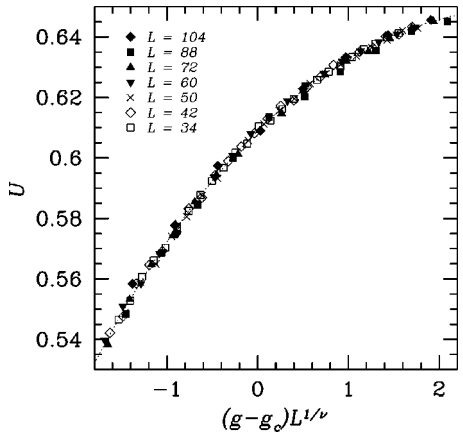

FIG. 12. Data collapse for the cumulant curves in the density map. The critical coupling found was $g_c=0.447\,15(18)$. The dotted line is the polynomial fitting.

TABLE I. Critical exponents for the threshold map, the density map, and the MH map with simultaneous updating. We include the exponents of the two-dimensional Ising model and the scale correction exponents (where needed) and the hyperscaling relations.

	Threshold map	Density map	MH map [1]	2D Ising
ν	0.921(22)	1.027(8)	0.887(18)	1.0
ω_ν		5.7(9)	1.5(4)	
β/ν	0.1257(43)	0.1255(20)	0.125(4)	0.125
ω_β	9.4(5)		9(4)	
γ/ν	1.741(11)	1.749(9)	1.748(10)	1.75
ω_γ			5.7(5)	
$(2\beta+\gamma)/\nu$	1.994(14)	2.000(98)	2.00(2)	2
β	0.1158(48)	0.1289(23)	0.111(5)	0.125
γ	1.603(34)	1.796(17)	1.55(4)	1.75

Moreover, the uniformity of the invariant distributions may actually not be an important factor, if we take into account that other maps, that are not piecewise linear, have already been located in the same universality class [1,7]. It is important to notice that the stochastic map we are considering is not simply a noisy version of the chaotic one. Here we have eliminated most of the deterministic nature of the dynamics, and only a Markovian feature is retained in that the signs of the variables are correlated.

We have also studied the reentrance phenomena found in these models, and have provided evidence of how strongly correlated they are with the appearance of antiferromagnetic clusters. These clusters are a consequence of simultaneous updating in a square lattice, where, for large couplings, half the lattice ''decides'' the future state of the other half, and vice versa. However, the results obtained show that even when antiferromagnetism is frustrated, some reentrance may remain. Therefore, it is clear that there should be some other factors that contribute to this behavior. As a possibility, it may happen that the ferromagnetic effect of the diffusive coupling saturates for ϵ very close to 1, independently of which type of lattice geometry one uses.

Results for the critical exponents are summarized in Table I, where the exponents for the MH map were taken from Ref. [1]. Our results for the stochastic lattice are consistent with those of the chaotic deterministic lattice, within error bars, and clearly outside of the 2D Ising class. The results for β/ν and for γ/ν are consistent with those of the Ising model. This supports the proposal, made by Marcq *et al.*, that what we are finding here is a weak form of the 2D Ising universality class. Something quite unexpected is the fact that one of the stochastic maps, the density map, seems to fall into the Ising class. The value for ν is a bit above 1, but the error bar is not short enough as to make credible a non-Ising behavior. Besides, we should remember that this exponent needed some finite-size corrections. Accepting then that the behavior of this map is Ising-like, a possible explanation is that, since stochasticity has been increased in the density map (compared with the threshold one), some correlations may have been erased, inducing in this way an effect similar to that of nonsimultaneous updating, thus driving the dynamics into the Ising class.

So at this moment we are left with the following puzzle: there is enough evidence, given in Refs. [1,7] and in this paper, about the existence of dynamical systems that undergo continuous phase transitions under diffusive coupling in 2D space, with critical exponents close but not quite equal to those of the 2D Ising model. This in spite of the fact that the symmetries of the models lead one to expect full compliance with the Ising universality class. However, not all maps with these characteristics fall outside of the Ising class, as shown by the case of the density map explored here. It seems therefore that something in the deterministic part of the dynamics induces extra correlations that push the model out of the Ising class. At the moment this remains unexplained.

There is a recent result that makes this result even more puzzling. It has been shown by Egolf [15] that under coarse graining, the diffusive lattice with local MH dynamics shows detailed balance and a Gibbsian measure, from where one can infer a Hamiltonian whose couplings flow in the manner expected for the Ising class. This result then would require the normal Ising exponents for the MH model, a thing that as we have mentioned just does not happen. One may perhaps assume that, since coarse graining is the starting point in Egolf's work, his results imply that some far-reaching finite size corrections are at play. The results gathered up to now do not give any indication of how this may be.

ACKNOWLEDGMENTS

We wish to thank H. Chaté for his useful comments. F.S. would like to thank the CONACyT. This work was supported by CONACyT through Grant No. 28383E.

[1] P. Marcq, H. Chaté, and P. Manneville, Phys. Rev. Lett. **77**, 4003 (1996); Phys. Rev. E **55**, 2606 (1997).
[2] H. Chaté and P. Manneville, Europhys. Lett. **14**, 409 (1991); **17**, 291 (1992).
[3] K. Kaneko, Chaos **2**, 279 (1992), and other articles in this special *focus issue* on coupled map lattices.
[4] J. Miller and D. Huse, Phys. Rev. E **48**, 2528 (1993).
[5] C. S. O'Hern, D. A. Egolf, and H. S. Greenside, Phys. Rev. E **53**, 3374 (1996).
[6] G. Grinstein, C. Jayaprakash, and Y. He, Phys. Rev. Lett. **55**, 2527 (1985); T. Bohr, G. Grinstein, Y. He, and C. Jayaprakash, *ibid.* **58**, 2155 (1987).
[7] D. Makowiec, Phys. Rev. E **60**, 3787 (1999).
[8] C. Boldrighini, L. A. Bunimovich, G. Cosimi, S. Frigio, and A. Pellegrinotti, J. Stat. Phys. **80**, 1185 (1995).
[9] F. Sastre and G. Pérez, Phys. Rev. E **57**, 5213 (1998).
[10] K. Binder, Z. Phys. B **43**, 119 (1982); K. Binder and D. Stauffer, in *A Simple Introduction to Monte Carlo Simulation and Some Specialized Topics*, edited by K. Binder, Applications of the Monte Carlo Method in Statistical Physics, Topics in Current Physics Vol. 36 (Springer-Verlag, New York, 1984).
[11] G. Vichniac, Physica D **10**, 96 (1984).
[12] B. Hayes, Am. Sci. **88**, 384 (2000).
[13] *Finite-Size Scaling and Numerical Simulation of Statistical Systems*, edited by V. Privman (World Scientific, Singapore, 1990).
[14] K. Binder, Rep. Prog. Phys. **60**, 487 (1997).
[15] D. A. Egolf, Science **287**, 101 (2000).